S. V. Hoeye, M. Fernández, L. Alonso, C. V. Antuña, P. Ghekiere and J. A. Casas, "A Novel Surface-Independent Textile Fully Woven UHF RFID Tag," in *IEEE Transactions on Antennas and Propagation*, vol. 70, no. 11, pp. 10156-10165, Nov. 2022, doi: 10.1109/TAP.2022.3191159.

A Novel Surface-Independent Textile Fully Woven UHF RFID Tag

Samuel Ver Hoeye, *Member, IEEE*, Miguel Fernández, Leticia Alonso, Carlos Vázquez Antuña, Pascal Ghekiere, and Javier Ardura Casas

***Abstract*— In this work, a UHF broadband surface-independent textile fully woven radio frequency identification (RFID) tag is presented. The antenna is composed of two stacked multilayer fabric pieces in which the shaped conductive and dielectric surfaces are part of the woven structure. In addition, a novel technique for the integration of the RFID chip in the woven structure was developed, providing a maximum integration level and making possible the manufacturing of the tag in a single step using conventional machinery from the textile industry. A tag prototype was experimentally characterized, showing a 12.5 m read range under a ±60 × ±60° angular range, when using a circularly polarized interrogator device with 35.2 dBm EIRP.**

***Index Terms*— Antenna, radio frequency identification (RFID) tag, textile technology.**

I. Introduction

THE number of applications based on the radio frequency identification (RFID) technology [1] has experimented an exponential growth in the last years. They are present in a large variety of sectors and fields, such as digital identity management, healthcare [2], [3], access control [4], or smart building [5]. Among all of them, RFID technology is especially attractive for the logistics sector because of its applications in warehouse management, tracing, and tracking systems [6]–[8].

Several frequency bands, including LF, HF, UHF, microwave, and, even, millimeter wave ranges [9], have been proposed to develop RFID applications, with very different technical characteristics and performance. In this way, when working in the LF and HF bands, the tags are usually based on loop antennas, which are magnetically coupled to the reader, providing very short detection ranges, with the maximum around a few centimeters. On the other hand, if UHF or higher frequency bands are selected, the communication between the tag and the reader is established through a conventional radio link, and the reading range can be as large as tens of meters, making these frequency bands specially suited for contactless monitoring and tracking applications. For these cases, a wide variety of antennas with different sizes, shape, and radiation characteristics is available, including folded [10] and bow-tie [11] dipoles printed over paper substrates, folded monopoles over conventional microwave substrates [12], 3-D printed wideband structures over PLA [13], and more complex tunable antennas [14]. Although the folded dipole approach is the most commonly used alternative, it must be taken into account that these structures are very sensitive to the underlying material, which can considerably degrade the antenna performance. Several different approaches have been proposed to address this issue, including the use of radiating elements over a ground plane [15], antennas specifically designed to operate over a metallic surface [16], or the use of high dielectric permittivity substrates [17], among some others. Although all of them are easily implementable using conventional electronic techniques, their main drawback related to this work is that their structure is not compatible with a woven implementation. In addition, in the cases in which the antenna does not include a ground plane, the performance of the tag is still dependent on the tagged material.

On the other hand, a different approach based on the use of textile antennas has attracted large research interest during the last few years. Textile antennas and, thus, derived RFID tags exhibit some particular characteristics as lightness, flexibility, and ease of integration in textile items, which makes them a very attractive alternative for a large variety of wearable RFID applications. Several different techniques for the implementation of textile antennas have been reported, including embroidering with conductive threads on fabric substrates [18]–[20], printing with conductive ink on fabrics [21], stacking several shaped conductive and dielectric fabric pieces [22]–[27], and using a single conductive thread as a dipole structure [28]. These textile RFID tags have been used in generic wearable applications [21], [22], [24], [25], human activity tracking [18], [23], and moisture [20], temperature [28], and deformation [19] sensing. In all of them, with the exception of [28], the RFID chip is attached to

Manuscript received 14 February 2022; revised 6 June 2022; accepted 29 June 2022. This work was supported in part by the European Commission EUROSTARS Program under Grant E!11802; in part by the MCIN/AEI/10.13039/501100011033/FEDER under Project PID2021-126301NA-I00 and Project EQC2019-005768-P; in part by the Gobierno del Principado de Asturias (PCTI) and FEDER under Project AYUD/2021/51706, Project IDI/2016/000372, Project IDI/2017/000083, Project IDI/2018/000191, and Project IDI/2021/000207; and in part by the Oviedo University under Project GR-2010-0015. *(Corresponding author: Miguel Fernández.)*

Samuel Ver Hoeye, Miguel Fernández, Leticia Alonso, and Carlos Vázquez Antuña are with the Department of Electrical Engineering, University of Oviedo, 33204 Gijón, Spain (e-mail: fernandezgmiguel@uniovi.es).

Pascal Ghekiere is with 3D Weaving, 8540 Deerlijk, Belgium (e-mail: pascal@3dweaving.com).

Javier Ardura Casas is with Wearable Technologies S. L., 33203 Gijón, Spain (e-mail: javier@wetech.es).

Color versions of one or more figures in this article are available at https://doi.org/10.1109/TAP.2022.3191159.

Digital Object Identifier 10.1109/TAP.2022.3191159

the textile structure using conductive epoxy resin, providing a moderate or poor integration level, and limited robustness against deformation and washing cycles [26], [27]. Furthermore, most of the cited works are based on radiating structures similar to dipoles, whose performance is strongly conditioned by the characteristics of the material on which they are placed.

In addition to the cited textile implementation options, a fully woven alternative has recently been demonstrated. This technology was applied to the design of microwave waveguides [29] and frequency selective surfaces [30], [31], low-frequency RFID tags [32], and microwave antennas [33], [34].

In this work, a textile UHF RFID tag based on a novel fully woven antenna is presented. The structure of the antenna was conceived to simultaneously provide adequate radiation pattern and bandwidth, ease of impedance matching and integration with the RFID chip, and performance independent on the tagged surface, while being compatible with a production process based on conventional techniques and machinery from the textile industry. Furthermore, a new technique to integrate the RFID chip in the woven structure at the weaving stage was developed, providing a maximum integration degree and allowing large-scale production.

This article is organized as follows. A general view of the tag is provided in Section II, while Section III describes in detail the textile structure. Section IV presents the electromagnetic modeling procedure and the simulation results. The technique developed to integrate the RFID chip with the woven structure is covered in Section V. Finally, the experimental results, both in laboratory and anechoic conditions, are shown and discussed in Section VI.

II. System Description

Fig. 1 schematizes the proposed tag. It is composed of a textile fully woven antenna based on a center-fed radiating slot opened on a rectangular cavity. A conductive strip is added under the slot as a part of the technique used to match the input impedance of the antenna with that of the chip.

The textile structure of the antenna consists of two stacked multilayer pieces in which all the shaped dielectric and conductive layers are part of the woven structure. Both fabric sheets are attached together with seams made with dielectric thread along several parallel lines (not represented in the figure for the sake of its clarity) aligned with the direction of the radiating slot. The two outer sewing lines were made with conductive threads to provide electrical connection between the top and the bottom faces of the antenna.

The broadband RFID chip model UCODE 7 SL3S1024, from *NXP*, was selected because of its broadband nature and its read sensitivity, around $P_{min} = -21$ dBm, which makes it suitable for long read range applications. It is connected at the center of the antenna between the two edges of the radiating slot, as indicated in Fig. 1. The chip input capacitance is $C_i = 0.63$ pF, providing an input impedance value, which varies from $Z_c = 14.5 - j293\ \Omega$ at 866 MHz to $Z_c = 12.5 - j267\ \Omega$ at 953 MHz. In this work, a discrete series inductor has been used to compensate for the imaginary part of Z_c at the working

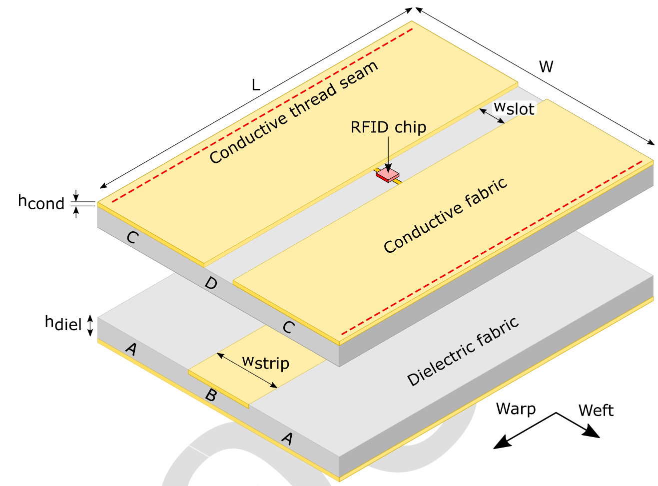

Fig. 1. Schematic of the proposed RFID tag. The dielectric fabric layers are represented in gray, whereas the conductive layers are colored in yellow. The red dashed lines indicate the conductive seams that holds together both fabrics and provides electrical contact between the top and the bottom faces of the antenna. Capital letters from “A” to “D” are used to identify the different sections, depending on their thread structure.

frequency. In combination with the conductive strip added under the radiating slot, this technique avoids the necessity of a large or complex additional matching network, easing the integration of the RFID chip with the antenna. Further details will be provided in the following sections. AQ:7

III. Textile Antenna Structure

Since the two multilayer fabric pieces which are part of the antenna were conceived to be implemented in an industrial loom, they are composed of warp and weft threads, which are perpendicular to each other. The warp threads are aligned with the length of the fabric, and they have to be previously mounted in the loom, whereas the weft threads are aligned with the width of the fabric, and they are added during the manufacturing process.

In this work, the conductive textile layers are implemented with *ELITEX 117/f17 2ply* threads. Each thread is formed by two twisted yarns, each with 17 filaments. The filaments are extruded from polyamide, and they are silver coated, with 1 μm thickness, providing a linear resistance around 70 Ω/m. The total linear density is 234 dtex, which indicates the weight in grams of a 10 km length of thread. On the other hand, the dielectric textile layers are implemented using polyester threads composed of two twisted multifilament yarns, and with 334 dtex linear density.

A. Bottom Fabric

The structure of the bottom multilayer fabric is schematized in Fig. 2. It is composed of two woven layers separated by five unwoven dielectric layers. The composition of the woven layers depends on the section, as indicated in Fig. 1. The bottom layer is made with conductive threads, and it is continuous along the three sections, since it forms the conductive bottom face of the antenna. Regarding the woven top layer, its

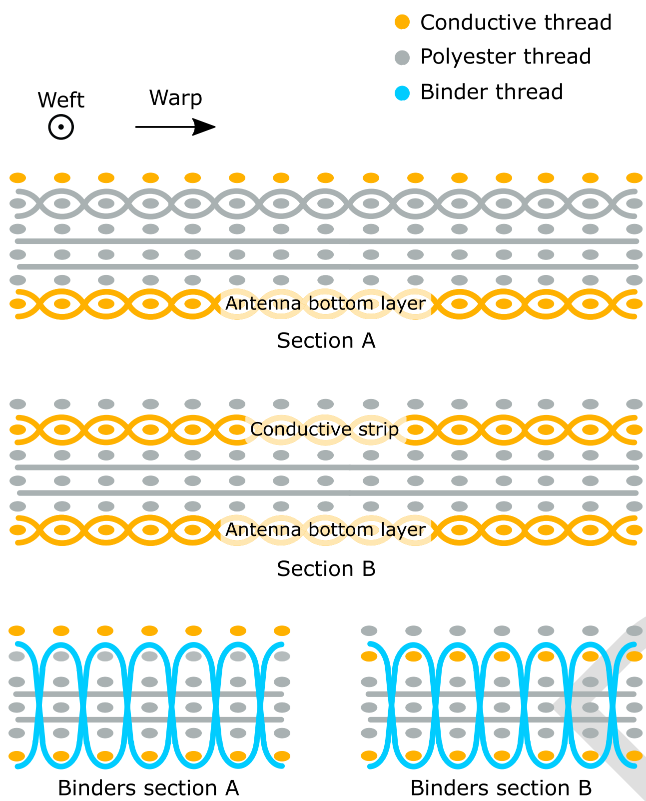

Fig. 2. Thread structure of the bottom multilayer fabric. The two top subfigures represent the conductive and dielectric layers, depending on the sections shown in Fig. 1. The two bottom subfigures show the binder threads location. In this case, the woven warp threads are not represented for the sake of the clarity.

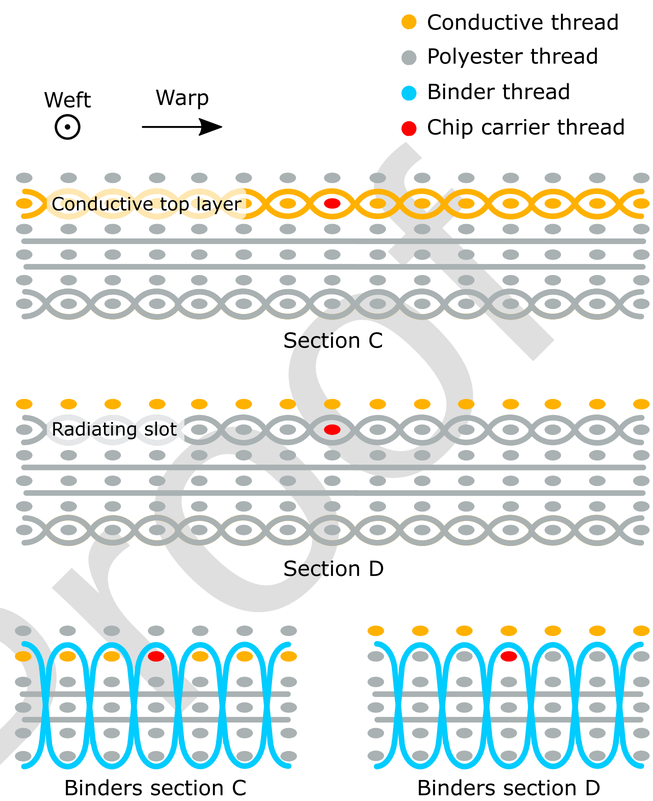

Fig. 3. Thread structure of the top multilayer fabric. The two top subfigures represent the conductive and dielectric layers, depending on the sections shown in Fig. 1. The two bottom subfigures show the binder threads location. In this case, the woven warp threads are not represented for the sake of the clarity.

central section, labeled as B, is made of conductive threads, as it implements the metallic strip under the radiating slot. On the other hand, the two sections labeled as A and located at both sides of the central one are implemented using dielectric threads. Finally, all the layers are held together using dielectric binder threads, as represented with blue color in Fig. 2.

The following consideration has to be taken into account. Since the top and the bottom fabrics are manufactured in an industrial loom as continuous pieces, the loom must be previously set up to be able to implement the different sections of each fabric piece and to automatically make the transition between sections without discontinuity. Thus, Fig. 2 represents the thread structure as it is used in the loom. In this way, the conductive weft threads located at the top of section A are used at section B to implement the conductive layer under the radiating slot, and those unused at section B are later cut and removed. In the same way, the dielectric threads located at the top of section B are moved up at section A to weave the dielectric layer, and then, the unused ones are removed from the fabric.

B. Top Fabric

Fig. 3 represents the thread structure of the top multilayer fabric. As in the case of the bottom fabric, it is manufactured as a single piece, and the loom must be set up to be able to weave the transition between the different sections, without creating any discontinuity. The fabric is composed of two woven layers separated by five dielectric unwoven layers, which are held together using dielectric binder threads. The lower woven layer is made with dielectric threads, and it is continuous through all the sections, while the composition of the upper woven layer depends on the section. The central section, labeled as D in Fig. 1, corresponds to the radiating slot, and therefore, it is implemented with dielectric threads. On the other hand, the sections labeled as C and located at the two sides of the central region are made of conductive threads, since they form the conductive top layer of the antenna.

IV. Electromagnetic Modeling and Simulation

This section describes the electromagnetic modeling and the simulation strategies carried out to calculate the impedance matching and the radiation characteristics of the proposed textile antenna.

A. Electromagnetic Modeling

From Figs. 2 and 3, it can be derived that the geometrical structure of the fabric is relatively complex. Furthermore, each thread is composed of several filaments. Therefore, modeling that the fabric structure in an EM simulator is a demanding task, and solving it requires a high-density mesh, leading to a computationally complex problem. Several strategies have been used to reduce the complexity of the model, while

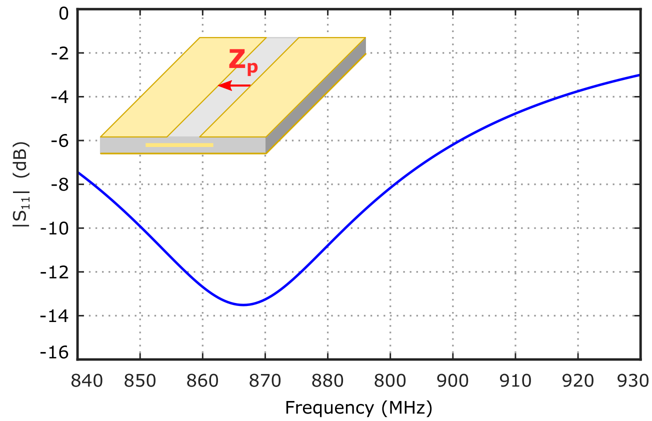

Fig. 4. Simulated reflection coefficient of the antenna. The reference impedance is $Z_p = 14.5\ \Omega$.

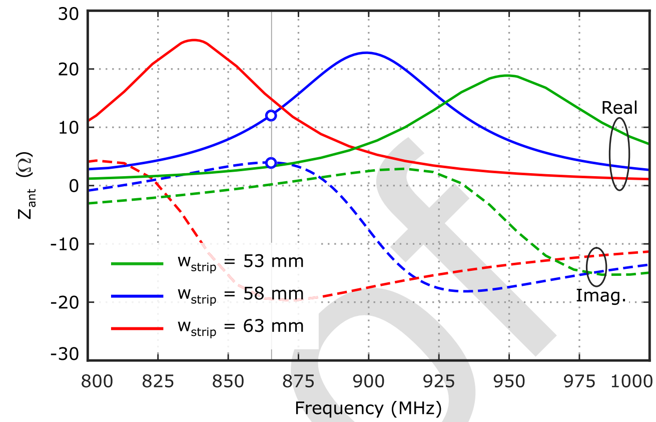

Fig. 5. Simulated antenna input impedance. Continuous trace: real part. Dashed trace: imaginary part.

maintaining an accurate representation of the EM behavior of the structure [35], [36]. The goal of the simplification procedure is to model each textile layer, either conductive or dielectric, as a homogeneous layer with equivalent EM behavior, but much easier to model and solve in commercial software than the original woven structure.

The equivalent model for the dielectric layers consists in a homogeneous layer with the same thickness h_{diel} as the original textile layer. The equivalent dielectric permittivity value $\varepsilon_{r,eq}$ is reduced with respect to that of the polyester from which the threads were extruded. This dielectric permittivity reduction is due to the air gaps contained in the structure of each thread and in the woven fabrics, as schematized in Figs. 2 and 3. The air percentage in each thread can be estimated from its linear mass density and the polyester density. On the other hand, the air percentage in the woven structure depends on the *epi* and *ppi* loom parameters, which indicate the number of warp and weft threads ends per inch. Here, the value of $\varepsilon_{r,eq}$ was experimentally estimated by implementing a substrate-integrated waveguide and measuring its cutoff frequency, obtaining a value $\varepsilon_{r,eq} \approx 1.82$.

Regarding the conductive layers, it should be taken into account that the conductive threads are obtained by applying a conductive coating to conventional dielectric threads. Due to the high density of the conductive fabric layers, numerous interconnections between warp and weft threads are made, allowing the current to flow in any direction. Thus, each conductive layer is modeled as an uniform layer with conductivity and thickness values similar to those of the filament coating, resulting in $h_{cond} = 1\ \mu$m and $\sigma_{eq} = 6.3 \times 10^7$ S/m.

B. Simulation Results

Once the layer model was obtained, the equivalent antenna structure can be easily modeled in an electromagnetic simulator to optimize it and to calculate the impedance mismatching with the RFID chip and its radiation characteristics. In this case, the ADS-momentum simulator from *Keysight*, based on the method of moments, was selected.

The impedance matching approach combines the optimization of the physical dimensions of the antenna with the use of a discrete coil with inductance $L_s = 53$ nH in series with the chip to compensate the imaginary part of its input impedance at the center frequency of the European UHF RFID band, 865–868 MHz. Thus, the input impedance of the series combination of the chip and the coil is $Z_{c,L} = Z_c + j\omega L_s \approx 14.5 - j4.4\ \Omega$ at 866.5 MHz. Then, to achieve conjugate impedance matching, the input impedance of the antenna Z_{ant} must be optimized to present a real part close to that of the chip, 14.5 Ω, and an imaginary part close to 0 Ω. This condition can be easily evaluated in a commercial simulator by calculating the antenna input reflection coefficient ρ_{ant} using a port with impedance $Z_p = 14.5\ \Omega$ located at the point at which the RFID chip will be connected, as indicated with a red arrow in the inset of Fig. 4. The calculated value of $S_{11} = 10\log_{10}(|\rho_{ant}|^2)$, referred to $Z_p = 14.5\ \Omega$, is represented in Fig. 4, showing the values under −10 dB between 850 and 880 MHz, which covers the European UHF RFID band, and indicating that the input impedance of the antenna Z_{ant} is close to the goal value. Outside the indicated frequency range, the antenna exhibits poorer performance, but, as will be shown in the next sections, it can still operate with a reduced read range.

On the other hand, Fig. 5 shows the simulated value of the antenna input impedance Z_{ant} for three different values of the strip width w_{strip}, providing $Z_{ant} \approx 12 + j4\ \Omega$ at 866 MHz for the optimum value of the strip width $w_{strip} = 58$ mm. The power transfer ratio τ between the antenna and the compensated chip can be calculated from

$$\tau = 4\frac{R_{c,L} R_{ant}}{|Z_{c,L} + Z_{ant}|^2} \tag{1}$$

where R_{ant} and $R_{c,L}$ are the real parts of the input impedance of the antenna and the compensated chip, respectively. The obtained result in this case is $\tau \approx 0.99$, indicating very low losses associated with the impedance mismatching.

From Fig. 1, the parameters to be optimized are the slot length L and width w_{slot}, the antenna width W, and the strip width w_{strip}. The thickness of the conductive and dielectric layers and the vertical location of the strip cannot be modified, since they depend on the fabric structure. The values of the optimized parameters are indicated in Table I, whereas the values of the dielectric permittivity of dielectric layers

TABLE I
OPTIMIZED VALUES OF THE GEOMETRICAL PARAMETERS

Parameter	Value (mm)	Parameter	Value (mm)
W	87.5	w_{strip}	58
L	128	h_{cond}	0.001
w_{slot}	5	h_{diel}	1.2

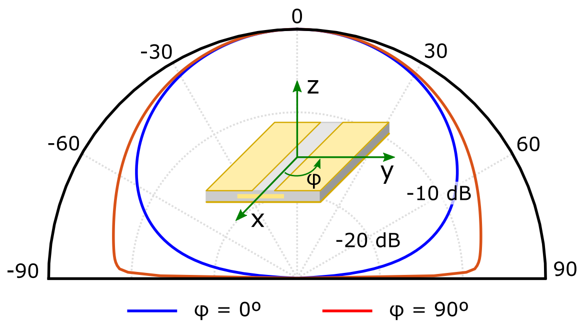

Fig. 6. $\varphi = 0^\circ$ and $\varphi = 90^\circ$ simulated radiation pattern cuts. The estimated radiation efficiency is $\varepsilon_{rad} \approx 7.5\%$, which provides a maximum gain value $G_{max} \approx -4.5$ dB in the $\theta = 0^\circ$ direction.

and the conductivity of conductive layers, which have been previously obtained in the described simplification process, are $\varepsilon_{r,eq} = 1.82$ and $\sigma_{eq} = 6.3 \times 10^7$ S/m.

Finally, Fig. 6 represents the simulated $\varphi = 0^\circ$ and $\varphi = 90^\circ$ radiation pattern cuts, evaluated at 866.5 MHz. The estimated radiation efficiency is $\varepsilon_{rad} \approx 7.5\%$, which in combination with the directive characteristics provides a maximum gain value $G_{max} \approx -4.5$ dB in the $\theta = 0^\circ$ direction. Note that the low efficiency value is mainly due to the reduced thickness of the dielectric layers and the relatively low conductivity of the conductive layers.

V. CHIP INTEGRATION

To enable the integration of the RFID chip with the antenna during the weaving process, the chip must be previously mounted on a carrier thread. To do that, a custom procedure, extending the technique reported in [37] and [38], was developed. Fig. 7 illustrates the main steps. First, a 50 μm polyimide strip was shaped, as shown in Fig. 7(a), and a 1 μm thick silver coating was deposited on the two narrow arms and on the indicated pads. Next, the chip and a series inductor, which is used to compensate the imaginary part of its input impedance at 866.5 MHz, were soldered at the central section and protected with epoxy resin [Fig. 7(b) and (c)]. Finally, a dielectric carrier thread was glued onto the back side of the polyimide piece, as shown in Fig. 7(d).

In this way, the thread carrying the chip can be managed by the loom as a conventional weft thread, as indicated in Fig. 3, and thus, the chip is integrated together with the textile antenna in the same weaving process. Note that the electrical connection between the chip terminals and the textile antenna is made through the direct contact between the silver coated arms of the polyimide piece and the conductive threads, which form the top layer of the antenna. In this way, it is flexible and provide a good robustness level against the deformation. On the other hand, it has been shown that enclosing the IC area in epoxy resin is one of the best alternatives to provide robustness against washing cycles and other stress sources [26]. Since that approach is used here, the whole tag is expected to exhibit an acceptable robustness level. Fig. 7(e) shows a picture of the chip mounted on the radiating slot.

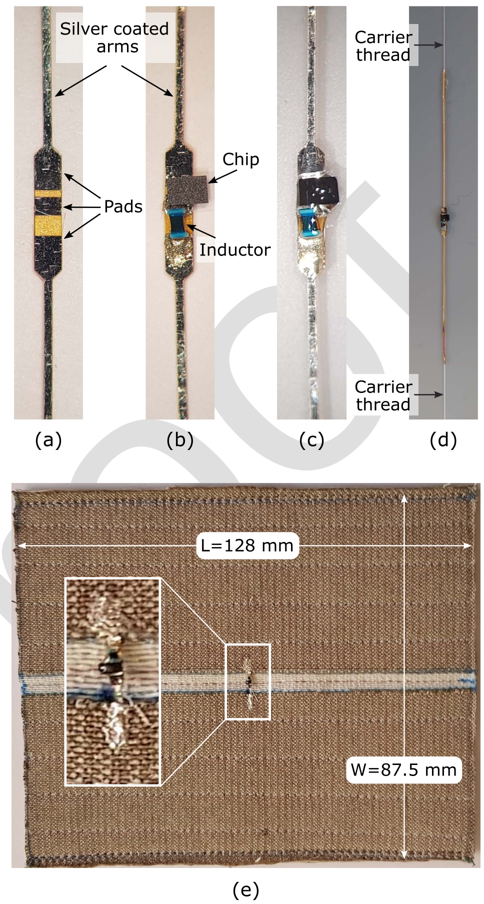

Fig. 7. Chip mounting procedure. (a) Polyimide piece with silver coated arms and pads. (b) RFID chip and inductor soldered. (c) RFID chip and inductor protected with epoxy resin. (d) Dielectric carrier thread glued onto the back side of the polyimide piece. (e) Picture of the manufactured RFID tag. Inset: magnification of the chip area.

The developed procedure has two additional advantages when compared with other mounting systems. The first one is that it allows to combine the textile antenna not only with RFID chips supplied together with the carrier thread, but also with virtually any RFID chip or, even, other small-form-factor integrated circuits, paving the way to the development of new applications based on textile antennas. The second advantage is related to the fact that the described procedure to mount the chip on the carrier thread requires relatively low cost equipment, especially if it is compared with other techniques as described in [28].

VI. EXPERIMENTAL RESULTS

The RFID tag was experimentally characterized in laboratory and in anechoic environments to determine its turn-on

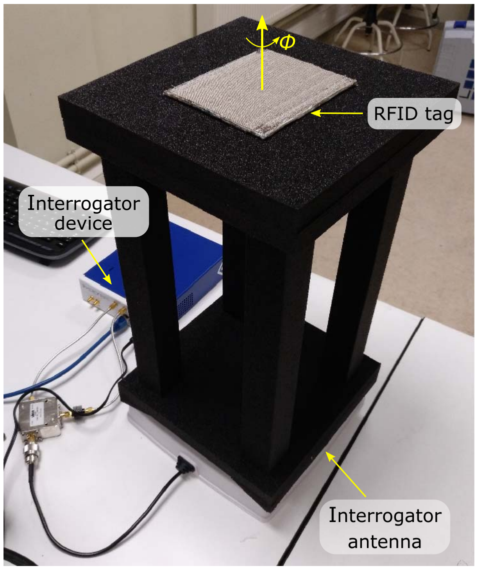

Fig. 8. Calibration and measurement setup. The RFID tag is over a 0.4 m height foam structure provided by the interrogator manufacturer to perform the calibration and the measurements.

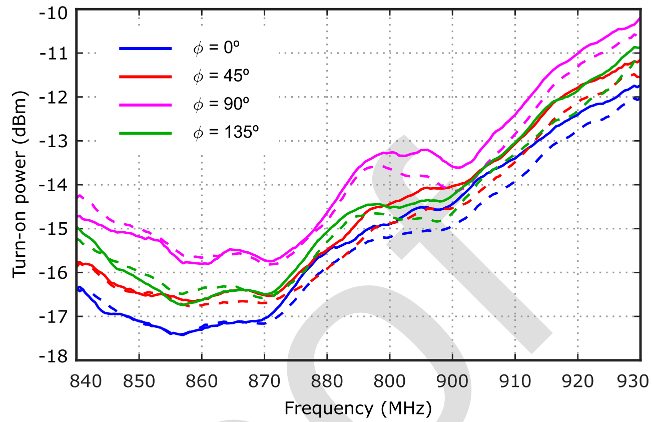

Fig. 9. Turn-on power for different rotation angles. Continuous trace: tag on air. Dashed trace: tag on metallic surface.

power P_{top}, the maximum reading distance d, and the radiation characteristics of the textile antenna. Furthermore, the performance of the tag under different deformation conditions was also tested. For the laboratory measurements, a monostatic setup based on the commercial interrogator device *Xplorer* from *CISC RFID* was used, combined with a circularly polarized antenna, providing a maximum 35.2 dBm EIRP.

A. Non-Anechoic Environment

The monostatic measurement setup represented in Fig. 8 was used to estimate the turn-on power and the reading range of the tag. In addition, the dependence of these parameters on the signal polarization and on the material on which the tag is placed was also evaluated. The setup is proposed by the interrogator manufacturer and consists of a foam structure, which holds the tag under test at 0.4 m distance from the interrogator antenna. Before performing the measurements, a calibration procedure is required. When performing the calibration, the performance of a reference RFID tag located at 0.4 m distance is evaluated and compared with recorded data obtained in a controlled environment. In this way, the effects of the current measurement scenario, which might perturb the results, can be mitigated.

The turn-on power P_{top} indicates the minimum value of the power available at the port of an ideal isotropic antenna located at the same place as the tag, required to activate the RFID chip. It is calculated by the interrogator by sweeping the transmitted power and taking into account the free-space propagation losses at a 0.4 m distance. Fig. 9 represents the obtained results for different tag rotation angles ϕ around its normal direction, when placing the tag on air and on a metallic surface. The difference between the measured turn-on power and the sensitivity of the RFID chip, $P_{min} = -21$ dBm, can be interpreted as a loss factor, which combines the gain of the textile antenna and the impedance mismatch with the chip. Note that the global performance of the tag makes it suitable to be used in the lower part of the considered frequency band, and that, at the best frequency point, around 860 MHz, the indicated loss factor is around 4 dB, which is in good agreement with the simulated gain and impedance mismatch. On the other hand, from the represented data, it can be concluded that the tag performance is not affected by the material on which it is placed. Finally, the less than 2 dB variation with the rotation angle for a given frequency value could be due to the moderate polarization purity of the interrogator antenna, which was not provided by the manufacturer.

From the turn-on power at the 0.4 m reference distance, the interrogator controller estimates the maximum reading distance d when working at the nominal 35.2 dBm EIRP by directly applying the Friis equation

$$d = \frac{\lambda}{4\pi}\sqrt{\frac{EIRP \cdot g_{RX} \cdot \tau}{P_{min}}} = \frac{\lambda}{4\pi}\sqrt{\frac{EIRP}{P_{top}}} \qquad (2)$$

where g_{RX} is the gain of the tag antenna, τ represents the power transfer ratio between the antenna and the chip, and $P_{min} = -21$ dBm is the chip sensitivity. P_{top} is the measured tag turn-on power when using the actual antenna, and it takes into account the antenna gain, the impedance mismatching, and the chip sensitivity. The result provided by the interrogator device is represented in Fig. 10, together with the value calculated from (2), showing a 13 m maximum reading distance around 860 MHz, while the value obtained for the European UHF RFID band (865–868 MHz) is around 12.5 m. Since this parameter is strongly related to the chip turn-on power, the same conclusions are valid. Nevertheless, note that the developed RFID tag provides a reading range over the whole frequency band, which makes it suitable for tracking applications, and that its performance does not depend on the material on which it is placed.

The performance of the prototype under different curvature conditions was also tested. The shape of the tag was adapted to the surface of two cylinders with radius $R = 30$ and $R = 20$ mm, and the reading distance was estimated as previously described. The measurement was performed with the radiating slot parallel and perpendicular to the cylinder

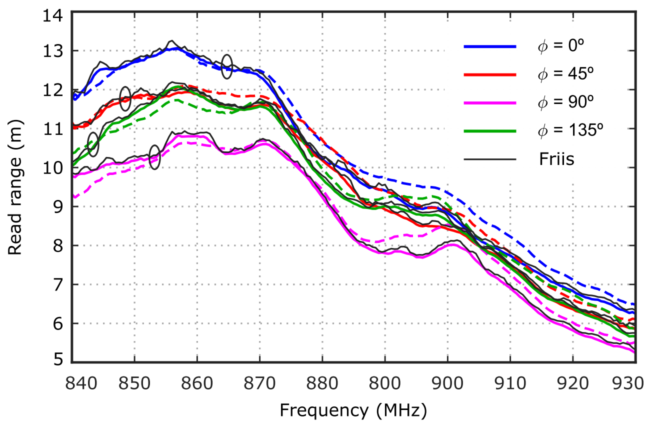

Fig. 10. Estimated reading range for different rotation angles. Continuous color trace: tag on air. Dashed color trace: tag on metallic surface. Continuous black trace: Friis equation.

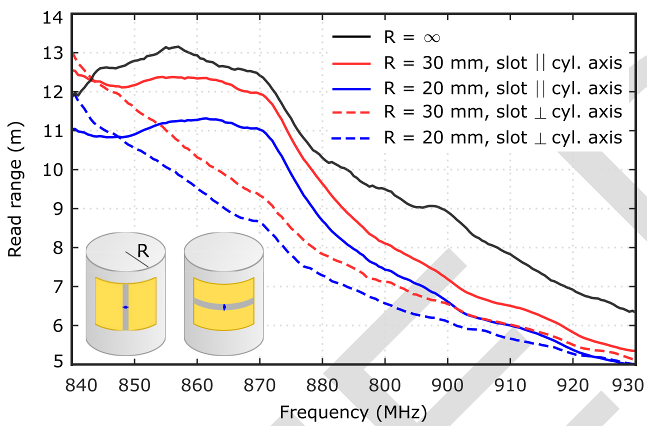

Fig. 11. Estimated reading range under different curvature conditions.

axis, as schematized in the inset of Fig. 11, which represents the obtained reading distance together with the reference trace obtained when the tag is not deformed. The performance is slightly degraded when deforming the antenna, but it still provides acceptable reading range values. Note that the setup in which the radiating slot is perpendicular to the cylinder axis provides the worst results, because, in this case, the distance between all the points along the radiating slot and the interrogator antenna is not constant, and therefore, the slot is illuminated with a nonuniform phase distribution.

B. Anechoic Environment

To characterize the radiation pattern of the textile antenna, the response of the RFID tag was analyzed in an anechoic chamber, as represented in Fig. 12. In this case, the tag was placed parallel to the interrogator antenna, at 4 m distance, and the $\varphi = 0°$ and $\varphi = 90°$ radiation pattern cuts were estimated from the backscattered modulated signal power $S(\theta)$ measured by the interrogator device. $S(\theta)$ represents the difference between the power of the side bands of the modulated signal generated by the RFID chip once it is excited and the power of the carrier, both of them evaluated at the interrogator location. Since $S(\theta)$ is generated by the RFID chip and radiated by

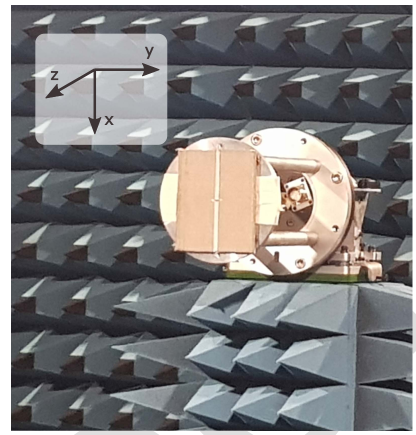

Fig. 12. RFID tag mounted in the anechoic chamber. The antenna is parallel to the XY plane.

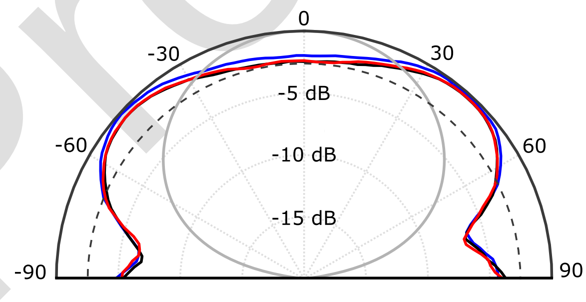

(a)

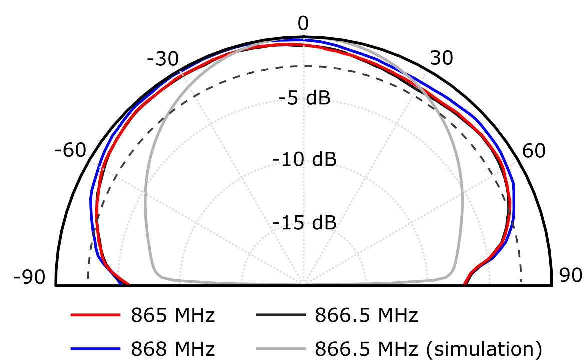

(b)

Fig. 13. Backscattered power $S(\theta)$ measured by the interrogator for different orientation angles. (a) $\varphi = 90°$ cut. (b) $\varphi = 0°$ cut. The black dashed trace at -2.5 dB indicates the normalized gain value in the $\varphi = 90°$ cut for the $\theta = 0°$ direction. It can be used to estimate the angular range under which the reading distance is larger than or equal to the 12.5 m nominal value.

the textile antenna, and it is independent on the power of the exciting carrier, its normalized value provides a good estimation of the radiation pattern of the antenna.

The obtained results are represented in Fig. 13, together with simulation data. To analyze them, note that the previously presented reading range was calculated for the $\theta = 0°$ direction. Thus, the reading range should be greater than or equal to that represented in Fig. 10 in the θ range for which $S(\theta) \geq S(\theta = 0°)$. Considering the $\varphi = 90°$ cut, because of the gain reduction observed around $\theta = 0°$, the

TABLE II
PERFORMANCE COMPARISON BETWEEN THE ACTUAL WORK AND PREVIOUSLY REPORTED TEXTILE UHF RFID TAGS

Ref.	Tech.	f (MHz)	Gain (dB)	Range (m)	Tx EIRP (dBm)
[20]	Embroidered	950	-	8	35.2
[21]	Printed	915	-	2.6	-
[22]	Attached fabrics	918	-7.1	5.8	-
[23]	Attached fabrics	866	-	1	28
[24]	Attached fabrics	868	-2.6	4.6	35.2
[25]	Attached fabrics	980	-	8	35.2
[28]	Single thread	860	-	6	-
This work	Woven	866.5	-4.5	12.5	35.2

previously presented read range values should be valid in the $-60 < \theta < 60°$ range. Similar conclusions can be extracted for the $\varphi = 0°$ cut, for which $S(\theta)$ presents a variation smaller than 1 dB in the range $-60 < \theta < 60°$. Finally, note that the frequency response of the antenna is flat in the considered 865–868 MHz range, which corresponds to the European RFID UHF band.

Finally, Table II compares the performance of the fabricated prototype with other textile RFID tags reported in the last three years. Most of them are implemented by attaching several single-layer conductive or dielectric fabric pieces together, and, with the exception of [28], the RFID chip is mounted using conventional techniques, providing low integration levels and robustness. Regarding the performance, this prototype exhibits the largest reading range described to date for a textile UHF RFID tag, to the best of the author's knowledge. Furthermore, this tag presents the maximum achievable integration level, since it is the only fully woven structure, including the chip.

VII. CONCLUSION

A novel textile fully woven UHF RFID tag capable of working over any material was presented. The textile antenna was accurately modeled in commercial EM software using previously reported techniques, and it was optimized to simultaneously achieve acceptable radiation properties and match the input impedance of the RFID chip, while avoiding the use of additional matching networks. A novel technique to mount the RFID chip and a lumped inductor on a carrier thread, which is then integrated in the woven structure, was developed. The proposed strategy provides a maximum integration degree, simplifies the implementation process, since the chip can be integrated with the textile structure at the weaving stage, and enables the use of virtually any integrated circuit with small form factor, paving the way for a large variety of applications based on textile antennas. A tag prototype was implemented and experimentally characterized, both in laboratory and in anechoic environments. The obtained results show that the tag can be detected in a 12.5 m range, under a $\pm 60 \times \pm 60°$ angular range, when working in the European RFID band, but it exhibits a minimum 6 m reading range in the 840–930 MHz frequency range, when using a circularly polarized interrogator device with 35.2 dBm EIRP. Furthermore, it is shown that the antenna can be placed on air and over a metallic surface without observing performance degradation. Finally, it is also demonstrated that the tag performance is still acceptable when curving it over a cylinder with radius comparable to the antenna dimensions.

REFERENCES

[1] K. Finkenzeller, *RFID Handbook: Fundamentals and Applications in Contactless Smart Cards and Identification*. Hoboken, NJ, USA: Wiley, 2003.

[2] S. S. Vedaei *et al.*, "COVID-SAFE: An IoT-based system for automated health monitoring and surveillance in post-pandemic life," *IEEE Access*, vol. 8, pp. 188538–188551, 2020, doi: 10.1109/ACCESS.2020.3030194.

[3] V. S. Naresh, S. Reddi, and N. V. E. S. Murthy, "Secure lightweight IoT integrated RFID mobile healthcare system," *Wireless Commun. Mobile Comput.*, vol. 2020, pp. 1–13, Mar. 2020, doi: 10.1155/2020/1468281.

[4] H.-W. Lee, "Design of multi-functional access control system," *IEEE Access*, vol. 9, pp. 85255–85264, 2021, doi: 10.1109/ACCESS.2021.3087917.

[5] S. Dey, R. Bhattacharyya, S. E. Sarma, and N. C. Karmakar, "A novel 'smart skin' sensor for chipless RFID-based structural health monitoring applications," *IEEE Internet Things J.*, vol. 8, no. 5, pp. 3955–3971, Mar. 2021, doi: 10.1109/JIOT.2020.3026729.

[6] K. Saito, "Proof of authenticity of logistics information with passive RFID tags and blockchain (extended abstract)," in *Proc. Int. Symp. VLSI Technol., Syst. Appl. (VLSI-TSA)*, Apr. 2021, pp. 213–216, doi: 10.1109/VLSI-TSA51926.2021.9440047.

[7] V. Hassija, V. Chamola, V. Gupta, S. Jain, and N. Guizani, "A survey on supply chain security: Application areas, security threats, and solution architectures," *IEEE Internet Things J.*, vol. 8, no. 8, pp. 6222–6246, Apr. 2021, doi: 10.1109/JIOT.2020.3025775.

[8] S. Gabsi, Y. Kortli, V. Beroulle, Y. Kieffer, A. Alasiry, and B. Hamdi, "Novel ECC-based RFID mutual authentication protocol for emerging IoT applications," *IEEE Access*, vol. 9, pp. 130895–130913, 2021, doi: 10.1109/ACCESS.2021.3112554.

[9] P. Burasa, T. Djerafi, N. G. Constantin, and K. Wu, "On-chip dual-band rectangular slot antenna for single-chip millimeter-wave identification tag in standard CMOS technology," *IEEE Trans. Antennas Propag.*, vol. 65, no. 8, pp. 3858–3868, Aug. 2017, doi: 10.1109/TAP.2017.2710215.

[10] M. T. Islam, T. Alam, I. Yahya, and M. Cho, "Flexible radio-frequency identification (RFID) tag antenna for sensor applications," *Sensors*, vol. 18, no. 12, p. 4212, 2018, doi: 10.3390/s18124212.

[11] L. Yang, A. Rida, R. Vyas, and M. M. Tentzeris, "RFID tag and RF structures on a paper substrate using inkjet-printing technology," *IEEE Trans. Microw. Theory Techn.*, vol. 55, no. 12, pp. 2894–2901, Dec. 2007, doi: 10.1109/TMTT.2007.909886.

[12] A. E. Abdulhadi and R. Abhari, "Design and experimental evaluation of miniaturized monopole UHF RFID tag antennas," *IEEE Antennas Wireless Propag. Lett.*, vol. 11, pp. 248–251, 2012, doi: 10.1109/LAWP.2012.2187632.

[13] G. A. Casula, R. Colella, L. Catarinucci, and Z. N. Chen, "A 3D-printed wideband antenna for UHF RFID," in *Proc. IEEE Int. Conf. RFID Technol. Appl. (RFID-TA)*, Pisa, Italy, Sep. 2019, pp. 384–386, doi: 10.1109/RFID-TA.2019.8892159.

[14] X. L. Chang, P. S. Chee, E. H. Lim, and N.-T. Nguyen, "Frequency reconfigurable smart antenna with integrated electroactive polymer for far-field communication," *IEEE Trans. Antennas Propag.*, vol. 70, no. 2, pp. 856–867, Feb. 2022, doi: 10.1109/TAP.2021.3111161.

[15] H.-D. Chen and Y.-H. Tsao, "Low-profile PIFA array antennas for UHF band RFID tags mountable on metallic objects," *IEEE Trans. Antennas Propag.*, vol. 58, no. 4, pp. 1087–1092, Apr. 2010, doi: 10.1109/TAP.2010.2041158.

[16] J. Zhang and Y. Long, "A novel metal-mountable electrically small antenna for RFID tag applications with practical guidelines for the antenna design," *IEEE Trans. Antennas Propag.*, vol. 62, no. 11, pp. 5820–5829, Nov. 2014, doi: 10.1109/TAP.2014.2354412.

[17] A. Ali Babar, T. Björninen, V. A. Bhagavati, L. Sydänheimo, P. Kallio, and L. Ukkonen, "Small and flexible metal mountable passive UHF RFID tag on high-dielectric polymer-ceramic composite substrate," *IEEE Antennas Wireless Propag. Lett.*, vol. 11, pp. 1319–1322, 2014, doi: 10.1109/LAWP.2012.2227291.

[18] Y. Liu *et al.*, "E-textile battery-less displacement and strain sensor for human activities tracking," *IEEE Internet Things J.*, vol. 8, no. 22, pp. 16486–16497, Nov. 2021, doi: 10.1109/JIOT.2021.3074746.

[19] M. Yu, X. Shang, M. Wang, Y. Liu, and T. T. Ye, "Exploiting embroidered UHF RFID antennas as deformation sensors," *IEEE J. Radio Freq. Identificat.*, vol. 4, no. 4, pp. 406–413, Dec. 2020, doi: 10.1109/JRFID.2020.3030790.

[20] X. Chen *et al.*, "Passive moisture sensor based on conductive and water-soluble yarns," *IEEE Sensors J.*, vol. 20, no. 18, pp. 10989–10995, Sep. 2020, doi: 10.1109/JSEN.2020.2994449.

[21] U. Hasni, M. E. Piper, J. Lundquist, and E. Topsakal, "Screen-printed fabric antennas for wearable applications," *IEEE Open J. Antennas Propag.*, vol. 2, pp. 591–598, 2021, doi: 10.1109/OJAP.2021.3070919.

[22] D. Le, S. Ahmed, L. Ukkonen, and T. Björninen, "A small all-corners-truncated circularly polarized microstrip patch antenna on textile substrate for wearable passive UHF RFID tags," *IEEE J. Radio Freq. Identificat.*, vol. 5, no. 2, pp. 106–112, Jun. 2021, doi: 10.1109/JRFID.2021.3073457.

[23] A. Mehmood *et al.*, "Body movement-based controlling through passive RFID integrated into clothing," *IEEE J. Radio Freq. Identificat.*, vol. 4, no. 4, pp. 414–419, Dec. 2020, doi: 10.1109/JRFID.2020.3010717.

[24] G. A. Casula, G. Montisci, and H. Rogier, "A wearable textile RFID tag based on an eighth-mode substrate integrated waveguide cavity," *IEEE Access*, vol. 8, pp. 11116–11123, 2020, doi: 10.1109/ACCESS.2020.2964614.

[25] Z. Khan *et al.*, "Glove-integrated passive UHF RFID tags—Fabrication, testing and applications," *IEEE J. Radio Freq. Identificat.*, vol. 3, no. 3, pp. 127–132, Sep. 2019, doi: 10.1109/JRFID.2019.2922767.

[26] S. Wang, N. L. Chong, J. Virkki, T. Björninen, L. Sydänheimo, and L. Ukkonen, "Towards washable electrotextile UHF RFID tags: Reliability study of epoxy-coated copper fabric antennas," *Int. J. Antennas Propag.*, vol. 2015, pp. 1–8, Nov. 2015, doi: 10.1155/2015/424150.

[27] R. B. V. B. Simorangkir, D. Le, T. Björninen, A. S. M. Sayem, M. Zhadobov, and R. Sauleau, "Washing durability of PDMS-conductive fabric composite: Realizing washable UHF RFID tags," *IEEE Antennas Wireless Propag. Lett.*, vol. 18, no. 12, pp. 2572–2576, Dec. 2019, doi: 10.1109/LAWP.2019.2943535.

[28] S. Benouakta, F. Hutu, and Y. Duroc, "Passive UHF RFID yarn for temperature sensing applications," in *Proc. IEEE Int. Conf. RFID Technol. Appl. (RFID-TA)*, Delhi, India, Oct. 2021, pp. 13–15, doi: 10.1109/RFID-TA53372.2021.9617438.

[29] L. Alonso-Gonzalez, S. Ver-Hoeye, M. Fernandez-Garcia, and F. L.-H. Andres, "Three-dimensional fully interlaced woven microstrip-fed substrate integrated waveguide," *Prog. Electromagn. Res.*, vol. 163, pp. 25–38, 2018, doi: 10.2528/PIER18040207.

[30] L. Alonso-González, S. Ver-Hoeye, M. Fernández-García, and F. L.-H. Andrés, "Broadband flexible fully textile-integrated bandstop frequency selective surface," *IEEE Trans. Antennas Propag.*, vol. 66, no. 10, pp. 5291–5299, Oct. 2018, doi: 10.1109/TAP.2018.2858141.

[31] L. Alonso-Gonzalez, S. Ver-Hoeye, M. Fernandez-Garcia, and F. L.-H. Andres, "Layer-to-layer angle interlock 3D woven bandstop frequency selective surface," *Prog. Electromagn. Res.*, vol. 162, pp. 81–94, 2018, doi: 10.2528/PIER18041707.

[32] L. Alonso-Gonzalez, S. Ver-Hoeye, C. Vazquez-Antuna, M. Fernandez-Garcia, and F. L.-H. Andres, "Multifunctional fully textile-integrated RFID tag to revolutionize the Internet of Things in clothing [wireless corner]," *IEEE Antennas Propag. Mag.*, vol. 61, no. 3, pp. 104–110, Jun. 2019, doi: 10.1109/MAP.2019.2907910.

[33] L. Alonso-Gonzalez, S. Ver-Hoeye, M. Fernandez-Garcia, Y. Alvarez-Lopez, C. Vazquez-Antuña, and F. L.-H. Andres, "Fully textile-integrated microstrip-fed slot antenna for dedicated short-range communications," *IEEE Trans. Antennas Propag.*, vol. 66, no. 5, pp. 2262–2270, May 2018, doi: 10.1109/TAP.2018.2814203.

[34] L. Alonso-Gonzalez, S. Ver-Hoeye, M. Fernandez-Garcia, C. Vazquez-Antuña, and F. L.-H. Andres, "On the development of a novel mixed embroidered-woven slot antenna for wireless applications," *IEEE Access*, vol. 7, pp. 9476–9489, 2019, doi: 10.1109/ACCESS.2019.2891208.

[35] L. Alonso-Gonzalez, S. Ver-Hoeye, M. Fernandez-Garcia, C. Vazquez-Antuña, and F. L.-H. Andres, "From threads to smart textile: Parametric characterization and electromagnetic analysis of woven structures," *IEEE Access*, vol. 7, pp. 1486–1501, 2019, doi: 10.1109/ACCESS.2018.2886041.

[36] L. Alonso-Gonzalez, S. Ver-Hoeye, C. Vazquez-Antuña, M. Fernandez-Garcia, and F. L.-H. Andres, "On the techniques to develop millimeter-wave textile integrated waveguides using rigid warp threads," *IEEE Trans. Microw. Theory Techn.*, vol. 66, no. 2, pp. 751–761, Feb. 2018, doi: 10.1109/TMTT.2017.2777983.

[37] M. Wagih, A. S. Weddell, and S. Beeby, "Sub-1 GHz flexible concealed rectenna yarn for high-efficiency wireless-powered electronic textiles," in *Proc. 14th Eur. Conf. Antennas Propag. (EuCAP)*, Copenhagen, Denmark, Mar. 2020, pp. 1–5, doi: 10.23919/EuCAP48036.2020.9136041.

[38] M. Wagih, Y. Wei, A. Komolafe, R. Torah, and S. Beeby, "Reliable UHF long-range textile-integrated RFID tag based on a compact flexible antenna filament," *Sensors*, vol. 20, no. 12, p. 3435, Jun. 2020, doi: 10.3390/s20123435.

Samuel Ver Hoeye (Member, IEEE) received the M.Sc. degree in electronics engineering from the University of Ghent, Ghent, Belgium, in 1999, and the Ph.D. degree from the University of Cantabria, Santander, Spain, in 2002.

He is currently an Associate Professor with the Department of Electrical and Electronic Engineering, University of Oviedo, Gijón, Spain. His research interests include the design and analysis of microwave, millimeter wave, and THz circuits and systems. Among these are the multifunctional oscillator-based circuits and antennas, frequency scanning antennas, graphene-based frequency multipliers and mixers, imaging systems, and textile integrated high-frequency components.

Miguel Fernández received the M.Sc. degree in telecommunication engineering, the M.Sc. degree in information technology and mobile communications, and the Ph.D. degree from the University of Oviedo, Gijón, Spain, in 2006, 2010, and 2010, respectively.

He is currently an Associate Professor with the Department of Electrical Engineering, University of Oviedo. His research interests include the design of microwave, millimeter wave, and THz circuits and systems. Among these are the multifunctional oscillator-based circuits and antennas, frequency scanning antennas, graphene-based frequency multipliers and mixers, imaging systems, and textile integrated high-frequency components.

Leticia Alonso received the M.Sc. degree in telecommunication engineering from the University of Oviedo, Gijón, Spain, in 2014, the M.Sc. degree in systems and control engineering from the Universidad Complutense de Madrid, Madrid, Spain, and the National University of Distance Learning (UNED), Madrid, in 2018, and the Ph.D. degree from the University of Oviedo in 2019. AQ:8

In 2017, she was a Visiting Scholar with the George Green Institute for Electromagnetics Research, University of Nottingham, Nottingham, U.K., where she was involved in the design, simulation, and manufacturing techniques to develop microwave and millimeter-wave passive circuits and antennas fully integrated in textile technology. Since 2014, she has been a Researcher with the Signal Theory and Communications Group, University of Oviedo.

Carlos Vázquez Antuña received the M.Sc. degree in telecommunication engineering, the M.Sc. degree in information technology and mobile communications, and the Ph.D. degree from the University of Oviedo, Gijón, Spain, in 2007, 2008, and 2013, respectively.

From 2007 to 2012, he was a Graduate Research Assistant with the Signal Theory and Communications Group, University of Oviedo, where he held different research and technical positions between 2012 and 2021, and has been an Assistant Professor since 2021. His research interests include the non-linear analysis and optimization techniques for the design of multifunctional oscillator-based circuits, antennas, and passive components, such as frequency multipliers and harmonic mixers, at microwave, millimeter/submillimeter-wave, and terahertz frequencies. In the last few years, he has been focused on the design of fully textile-integrated circuits and antennas, suitable for mass production using common processes in the textile industry.

Pascal Ghekiere received the M.Sc. degree in electronic engineering from the Howest University of Applied Sciences, Kortrijk, Belgium, in 1997.

He is currently the CEO of the high-tech SME 3D Weaving, Deerlijk, Belgium, where he is involved in the production of 3D woven fabrics, including distance fabrics, multilayers, tubular fabrics, or a combination in a more complex fabric. He is the owner of the brand SpacerGlass, a woven distance fabric, with many advanced applications, and he has been involved in the integration of active optical and microwave devices in fully woven 3D fabrics.

Javier Ardura Casas is the Founder and CEO of the high-tech SME Wearable Technologies S. L., Gijón, Spain, where he is involved in the design and development of wearable IoT products for the finance, health, industrial, and retail sectors.